

Can CNNs Construct Highly Accurate Model Efficiently with Limited Training Samples?

Yu Li^a, Hu Wang^a, Juanjuan Liu^a

a. State Key Laboratory of Advanced Design and Manufacturing for Vehicle Body, Hunan University, Changsha, 410082, PR China

Highlights

- CNN is applied to model high dimensional and strong nonlinear problems.
 - Different intervals, dimensions, and training sample sizes are considered.
 - Several highly nonlinear and dimensional mathematical functions are modeled.
 - CNN is applied to the optimization of complex geometric structure.
-

Abstract

It is well known that metamodel or surrogate modeling techniques have been widely applied in engineering problems due to their higher efficiency. However, with the increase of the linearity and dimensions, it is difficult for the present popular metamodeling techniques to construct reliable metamodel and apply to more and more complicated high dimensional problems. Recently, neural networks (NNs), especially deep neural networks (DNNs) have been widely recognized as feasible and effective tools for multidiscipline. Actually, some popular NNs, such as back propagation neural networks (BPNNs) can be regarded as a kind of metamodeling techniques. However, for high dimensional problems, it seems difficult for a BPNN to construct a metamodel. In this study, to construct the high accurate metamodel efficiently, another powerful NN, convolutional neural networks (CNNs) are introduced to construct metamodels. Considering the distinctive characteristic of the CNNs, the CNNs are considered to be a potential modeling tool to handle highly nonlinear and dimensional problems with the limited training samples.

Keywords: CNN; Metamodel; High dimension; Strong nonlinear; Small sample set

1. Introduction

At present, many engineering analyses ask the requirement of complicated analyses and calculation codes, e.g. finite element analysis (FEA). Despite the increasing of computers, the cost of manpower and material resources for calculation limit development. How to provide a computationally cheap code and how to solve the high-dimensional and strong nonlinear analyses efficiently and accurately have become unresolved hot spots of concern.

A popular method to solve the above issues is to apply a cheap approximate model to describe the complex analysis. And this approximate model, i.e. *metamodels*, provide a "model of the model" [1]. Mathematically, assume the input information is vector \mathbf{x} , and the output information is vector \mathbf{y} , the code actually calculates

$$\mathbf{y} = f(\mathbf{x}) \quad (1)$$

where $f(\mathbf{x})$ is the function for the real model. The function for the approximate model is

$$\hat{\mathbf{y}} = g(\mathbf{x}) \quad (2)$$

where

$$\mathbf{y} = \hat{\mathbf{y}} + \varepsilon \quad (3)$$

where ε includes both approximation and random errors.

Today, there are many metamodels help $g(\mathbf{x})$ approximate $f(\mathbf{x})$, i.e. polynomial response surface models (PRSMs), multivariate adaptive regression splines (MARSs), radial basis functions (RBFs), kriging interpolation (KI) and support vector regression (SVR) [2, 3]. However, it appears that few of them are powerful when modeling high-dimensional and strong nonlinear analyses.

In this study, deep neural networks (DNNs) is employed for complex analyses. In 2006, Professor Hinton [4], one of the founders of the deep learning (DL), through the analysis of human brain's decision making power, proposed to build deep neural networks (DNNs) by increasing the artificial neural networks (ANNs)' layers and the neurons of each layer. He started the wave of applications of DL and large data. Until 2017, the team *DeepMind* of Google published the latest research *Mastering the game*

of Go without human knowledge on nature. DNNs and large data have always gathered people's focus.

DNNs have a significant advantage for analysis of unstructured, unspecified patterns and cross-domain large data. Generally, the classical NNs can be classified into feedforward NNs and feedback NNs. The former has been applied widely for its strong ability of approximating nonlinear mappings [5-10]. The most popular feedforward NN is back propagation neural network (BPNN). The classical BPNNs [11] make full use of the advantage of multilayer forward network structure [12], and their algorithm is relatively mature. Infinite deep neural networks (IDNNs), i.e. recurrent neural networks (RNNs) [13], are dynamical systems essentially. Their essential character is that the states of the networks change with the time and couple the time. Hence they are suitable for extracting the features of the time. Radial basis function neural network (RBFNN) [14] is a special kind of single hidden layer NNs, which has a simple structure, and it is easily trained. Meanwhile, it is at present widely applied in engineering fields such as pattern recognition, target prediction and function interpolation [15]. Moreover, the RBFNN greatly reduces the training samples and improves the accuracy through continuous optimization from scholars, such as the changing width factor RBFNNs (CWF-RBFNNs) [16]. Adaptive wavelet neural networks (AWNNs) [17] which are combined with wavelet analysis (VA) make full use of the advantages of BPNNs and RBFNNs. Moreover, they have a faster convergence rate while overcome the RBFNNs' shortcoming of local minimal. Since, in many cases, the BPNN of one hidden layer or three layers is sufficient to analyze most problems [18-21], the BPNNs have become the preferred NN models.

BPNNs' characteristics are presented in Table 1. However, due to the bottleneck of their algorithms, the computationally expensive of computers and time consuming, the number of design variables is limited.

Table 1 Characteristics of the BPNN.

BPNNs	Characteristics
Advantages	i. Strong ability of non-linear mapping. ii. Higher capability of self-learning and self-adapt.

Shortcomings

- iii. Good generalization ability to adapt to a new sample.
 - iv. Strong fault tolerance.
 - i. A large number of necessary training samples.
 - ii. The convergence rate is slow.
 - iii. The training process has randomness, and it means that under the same configuration parameters, the training results may appear quite different.
-

For the characteristics mentioned above, we seek to provide another NN to construct a high-dimensional model. In this study, convolutional neural networks (CNNs) are considered. Commonly, CNNs are widely applied in image recognition, and the input variables are pixels of an image. Generally, if the image's pixel is $28 \times 28 = 784$, it means the input dimension to the CNN is 784. However, the input dimension may increase to million level for larger images such as 1024×1024 pixels. Surprisingly, in the field of image classification, CNN's accuracy is more than 95%. Therefore, CNN has its own advantages in analyzing high-dimensional problems. This is why we seek to employ the CNNs to analyze the high-dimensional (the input dimension is greater than 100) and strong nonlinear problems which are bottleneck for the aforementioned metamodels. In this study, we explore, evaluate and analyze CNN's capability (when modeling highly nonlinear and dimensional problems) and transfer learning from image recognition to engineering application. The remainder of this paper is organized as follows. The basic theories of BPNNs are summarized, and an evaluation scheme for BPNNs' ability is provided next. In Section 3, CNNs are applied to analyze the high-dimensional and strong nonlinear problems. In Section 4, the results of BPNNs and CNNs are compared and analyzed. After a series of observations and analyses, CNNs are applied to the optimization of the complex geometric structure in Section 5. The summaries are given in the final section.

2. Back propagation neural network

2.1. Overall framework

BPNN, which is the most widely employed model among the ANN models, was introduced by Rumelhart and McClelland [22] in 1986, and it is a kind of multi-layer feedforward neural networks (MFNNs). Its overall framework is shown in Fig. 1,

which consists of N layers including the input layer, several hidden layers and the output layer. The core characteristic of the BPNN is to feed back the error from output to the each layer's weight in order to correct each weight [23].

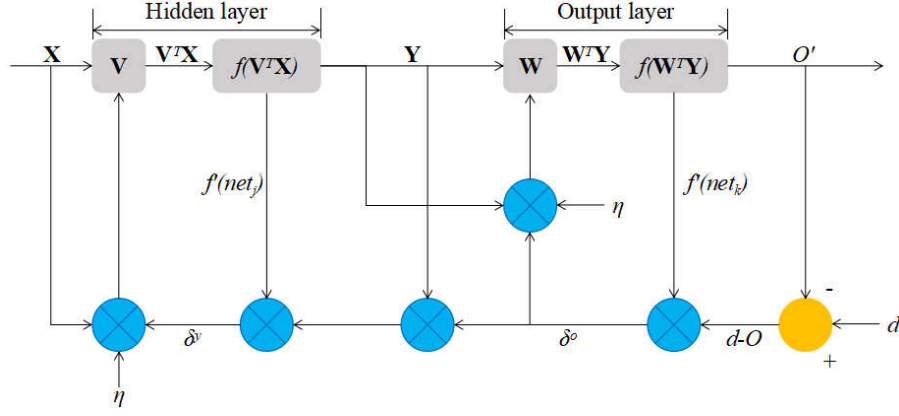


Fig. 1. Flow chart of BPNNs' signal.

(where \mathbf{X} is the input matrix, \mathbf{V} and \mathbf{W} are weight matrix, $f(x)$ is the activation function, $f'(x)$ is the derivative of the activation function, O is the prediction of BPNN and d is the actual value, δ^o is the gradient of error $d-O$ to \mathbf{W} and δ^v is the gradient of error $d-O$ to \mathbf{V} , and η is the learning rate.)

2.2. Application

There are following three aims should be taken into account about BPNN.

- I. What is the maximum input interval used in BPNNs?
- II. What is the maximum input dimension BPNN can model?
- III. What is the cost of training samples' preparation for BPNN?

2.3. A multidimensional case

In this section, we seek to apply the BPNN to a typical nonlinear multidimensional case. Because the Griewank function has many local maxima, the Griewank function is employed to test the BPNN's capability. The Griewank function shown in Fig. 2 is given by

$$f(x) = \sum_{i=1}^d \frac{x_i^2}{4000} - \prod_{i=1}^d \cos \frac{x_i}{\sqrt{i}} + 1 \quad (4)$$

where d is the number of design variables.

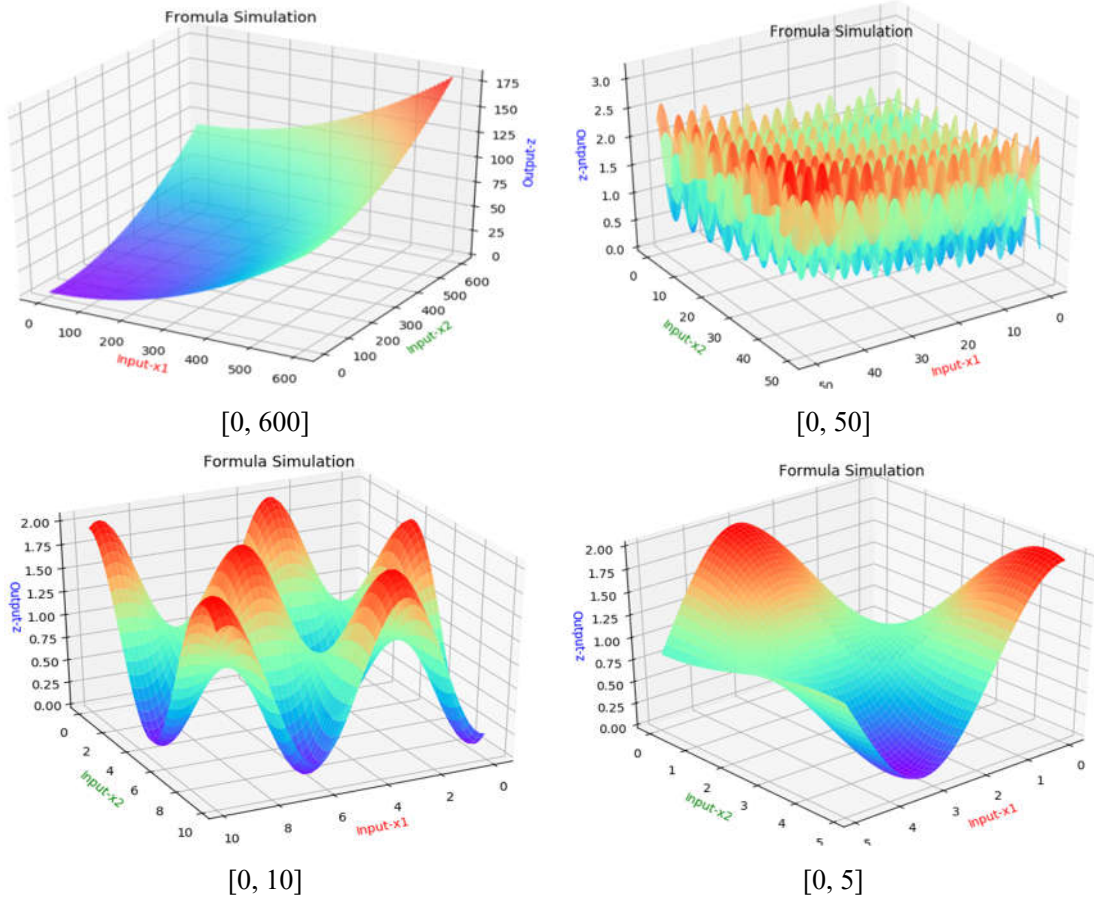


Fig. 2. The Griewank function.

In the classical BNPP, the Sigmoid function are usually employed as the activation functions in the input and hidden layers [24], while a linear function is employed as the output layer's. The Sigmoid function can be categorized into two groups based on whether the output value contains a negative: *Log-Sigmoid* function and *Tan-Sigmoid* function. The Log-Sigmoid function is employed to this study and is calculated by

$$f(x) = \frac{1}{1 + e^{-x}} \quad (5)$$

A feedforward neural network can construct the mapping between the input variables and the output value through iterative training. The *loss function* is employed to determine if the training should be terminated, and calculated by

$$total_losses = MSE(y, y') + \lambda R(w) \quad (6)$$

where

$$MSE(y, y') = \frac{\sum_{i=1}^n (y_i - y_i')^2}{n} \quad (7)$$

$$R(w) = \sum_i [\alpha |w_i| + (1 - \alpha) w_i^2] \quad (8)$$

where y_i is the actual value, y_i' is the predictive value, α is the proportion of L1 regularization to the total regularization, and n is the number of training samples.

Learning rate, usually, is designated initially as 0.7 [25], and subsequently adjusted according to the training process. In this study, a more flexible method is introduced to determine the learning rate -- *exponential decay method* (EDM):

$$\eta = \eta_0 \cdot \text{decay_rate}^{(\text{global_step} / \text{decay_step})} \quad (9)$$

where η_0 is the initial learning rate, *decay_rate* is the *attenuation coefficient*, *global_step* is the current step in the training process, and *decay_step* is the decay rate. In order to clearly master the accuracy of the trained model, the relative errors (REs) of the testing samples are shown to us and calculated by

$$RE = \left| \frac{y_i - y_i'}{y_i} \right| \quad (10)$$

If each RE value is close to 0, it indicates that the goodness-of-fit of the NN model is satisfied and the model has a strong capability.

The interval of each x_i is clustered into [0, 5], [0, 10], [0, 50], [0, 600] and dimension is to 2 to observe BPNNs' capabilities increased with the interval of each x_i , structural parameters of BPNN are shown in Table 2. Usually some rules are employed to determine the number of hidden layer's nodes.

- I. The number of hidden layer's nodes is 70% to 90% of the input layer's. [26]
- II. The number of hidden layer's nodes is less than twice of the input layer's. [27]
- III. The number of the hidden layer's nodes should be between the input and output layers'. [28]
- IV. The nodes of the first and second hidden layers should be approximately equal. [21]

Actually, the number of hidden layers and each layer's node are not absolutely certain. Therefore, we comply the rules mentioned above incompletely based on actual training process.

Table 2 The structural parameters of BPNN under different input intervals.

Interval	Number of hidden layers	Nodes' number of hidden layers		Training dataset size	Testing dataset size	RE
[0,5]	1	6		3000	100	≤30%
[0,10]	2	No.1	6	8000	100	
		No.2	6			
[0,50]	4	No.1	6	10000	100	
		No.2	8			
[0,600]	4	No.1	4	5000	100	
		No.2	8			
		No.3	8			
		No.4	6			

If the BPNN analyzed above is equipped with accuracy requirement, the BPNN can be used for further analysis. When the interval is set as [0, 100], the input dimension should be increased to test BPNN's capability increased with the input dimension. In this study, the dimensions of Griewank function are set as 5, 10 and 20, respectively. The structural parameters of the BPNN under different input dimensions are presented in Table 3.

Table 3 The structural parameters of BPNN under different input dimensions.

Dimension	Number of hidden layers	Nodes' number of hidden layers		Training dataset size	Testing dataset size	RE
5	3	No.1	10	5000	100	≤30%
		No.2	8			
		No.3	8			
10	3	No.1	20	8000	100	
		No.2	8			
		No.3	10			
20	4	No.1	8	14000	100	
		No.2	18			
		No.3	16			
		No.4	12			

As is known to all, with the increase of dimension and expand of interval, the number of necessary training samples increases rapidly. It is necessary to know the most reasonable number of training samples once the interval, dimension and the maximum RE are determined, in order to avoid wasting time of redundant training samples.

3. Convolutional neural network

It is well known to all that the more the NN's layers are, the stronger the NN is. However, it is difficult to get a "deep" BPNN by the gradient descent optimizer (GDO) because BPNN's gradient is difficult to exceed three layers. This is partly because BPNN's gradient is difficult to exceed three layers. Therefore, a "deep" BPNN's model is difficult to be achieved. What's more, when a BPNN is employed to model a high-dimensional problem, the critical problem is that a large number of training samples are commonly necessary, and a great deal of manpower and material resources for samples are consumed. At the same time, the parameters in a BPNN's full connection layer are too many. For example, if the input dimension is 900 and there are 500 nodes in the first hidden layer, then the full connection layer obtains $900 \times 500 + 500 = 450500$ parameters, where 500 additional parameters are the bias corresponding to each node. Moreover, too many parameters will easily cause the over-fitting problem. Therefore, a more reasonable and effective network structure for high-dimensional and strong nonlinear problems is demanded. In our opinion, the Convolutional Neural Network (CNN) [29, 30] might be a useful tool for analyzing the aforementioned problems, even the CNN is seldom applied to modeling.

Learning method of CNNs is the supervise learning (SL). Similar to the full connection NN, the CNN is composed through layers of nodes. And it has been applied widely, such as natural language processing [31-34], medical development [35], disaster discovery [36] and even the human intelligence program [37].

3.1. Overall framework

As shown in Fig. 3, the training and testing procedures of CNN are divided into three parts. Firstly, the training and testing samples are randomly generated in design interval. And then, each training sample is submitted to the CNN to generate a function approximation. At last, additional testing samples are applied to test the trained model's accuracy.

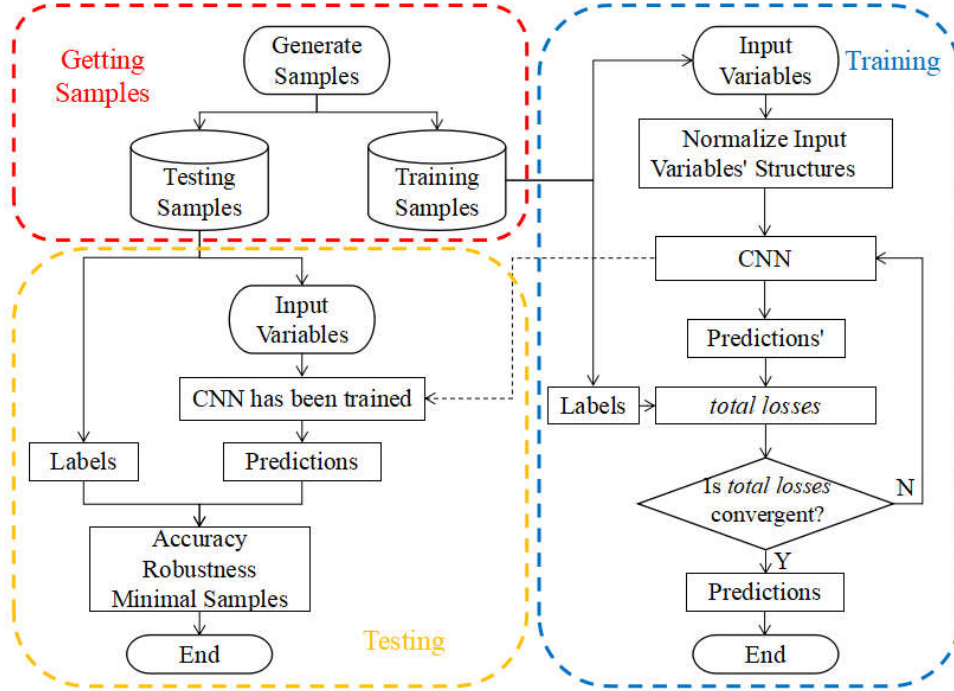


Fig. 3. The procedure of model construction using CNN.

There exists many CNN architectures, such as CifarNet [38, 39], AlexNet [30], GoogLeNet [40] and so on, and a more complex CNN models among them have only about 150K or 15K parameters [39, 41]. Where does CNN's capability come from when modeling high-dimensional and strong nonlinear problems? CNNs illustrated in Fig. 4 combine three properties [42, 43]:

- I. Local connection.** This is the most straightforward characteristic of CNNs. Each neuron is not connected to all neurons from the upper layer, but connected to a small part. This enable the model to reduce parameters effectively.
- II. Weight sharing.** Each network layer shares a same weight vector \mathbf{w}_i , rather than each local connection mentioned above has a different weight vector. This also reduces a lot of parameters.
- III. Local pooling.** The pooling layer is used to reduce each layer's nodes. It not only can reduce the CNN's parameters, but also can enhance the CNN's robustness.

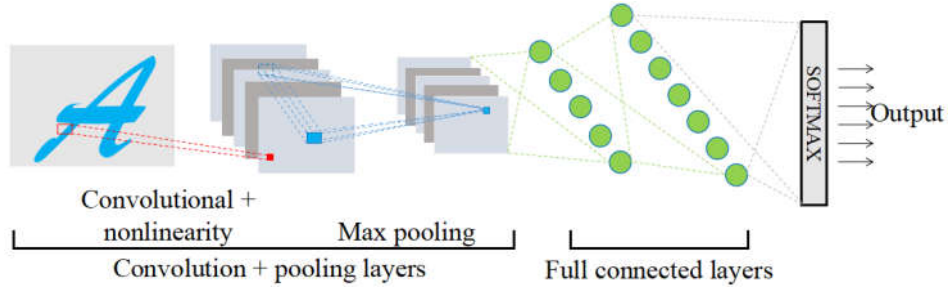


Fig. 4. Architecture diagram of a CNN.

The key features of the CNN architecture are described below:

- I. **Input layer.** The Input layer is the entrance to the whole CNN. It takes an image of pixels $W \times H \times 3$ (RGB image) or $W \times H \times 1$ (monochrome image) as input. Starting from this layer, the transfer vector of each layer is converted into a three-dimensional matrix.
- II. **Convolutional layer.** The convolutional layer is the most important part of a CNN. Compared with the classical full connection layer, the input to each node of a convolution layer is a small part from the upper layer's nodes. The convolutional layer analyzes each node's input to obtain a higher degree of abstract understanding.
- III. **Pooling layer.** The pooling layer reduces the computation for deeper layers while preserving the important activations.
- IV. **Full connection layer.** After several convolutional layers and pooling layers, it can be considered that the information of the input variables has been abstracted into a very high level. After feature extraction and analysis of the front layers, a full connection layer is still necessary to complete the model's construction.
- V. **Softmax layer.** The softmax layer is mainly used for the problems of classification, if the problem is regression, the softmax layer is not the essential element.

The forward propagation process of a convolutional layer mainly depends on a *filter* or a *kernel*. As shown in Fig. 5 and Eq. (11), where $\mathbf{a}_{x,y,z}$ is the feature vector at spatial location (x, y, z) in the input vector, $\mathbf{w}_{x,y,z}^c$ is the weight vector from c -th filter in a convolutional layer and \mathbf{b}_c is the bias vector, then the output from a filter is

$$g(x) = f\left(\sum_{i,j,k} (a_{x+i,y+j,z+k} * w_{i,j,k}^c + b_c)\right) \quad (11)$$

where * represents dot product.

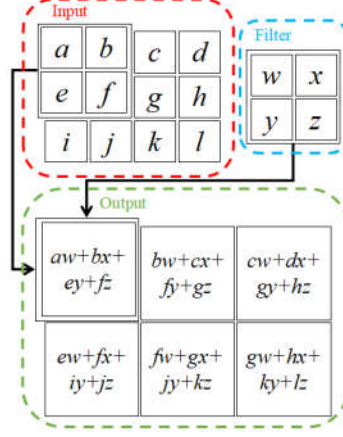


Fig. 5. The forward propagation process of the convolutional layers.

A pooling layer can reduce the size of the input matrix very effectively. The pooling layer can not only speed up the calculation, but also prevent the over-fitting problem. Similar to the convolutional layer, the forward propagation process of the pooling layer is done by moving a structure which is similar to a filter. However, the pooling layer's filter does not calculate the weighted sum of the input, but the maximum value or average value. The pooling layer, which calculates the maximum value, is the *maximum pooling*, and the pooling layer, which is averaged, is the *average pooling*.

3.2. LeNet-5

The model of CNN applied in this study is LeNet-5, which was developed by Yuan [44] in 1998. And better results has been achieved by the LeNet-5 in the image classification problem. As shown in Fig. 6, in order to apply the LeNet-5 to this study better, the architecture of LeNet-5 is optimized. Commonly, LeNet-5 is applied to classify images and the input variables are pixels of the image. When analyzing a high-dimensional mathematical problem, design variable vector is converted into a matrix of $M \times N \times 1$ which is similar to the distribution of a monochrome image's pixels. Then the matrix is regarded as a "monochrome image", and each design variable is regarded as an "image's pixel". At last LeNet-5 analyzes the "image". The key features of this LeNet-5 architecture are described in Table 4.

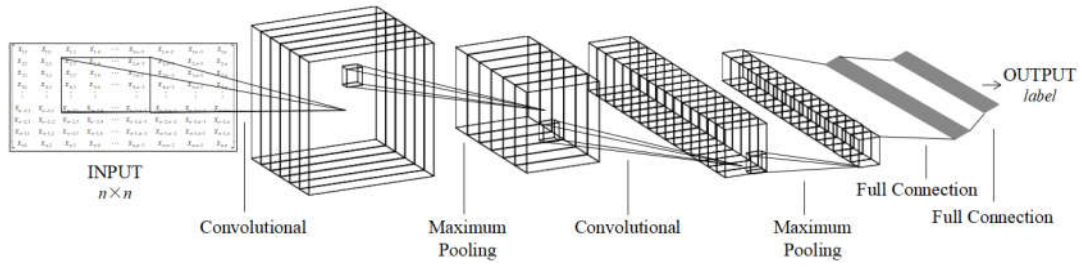


Fig.6. LeNet-5 of this study.

Table 4 LeNet-5 architecture used in this study.

Number of hidden layer	Type of layer	Parameter & characteristic
1 st	Convolutional layer	Size of filter 5×5, depth of filter is 32, moving step of filter is 1
2 nd	Pooling layer	Maximum pooling, length of filter is 2, moving step of filter is 2
3 rd	Convolutional layer	Size of filter 5×5, depth of filter is 64, moving step of filter is 1
4 th	Pooling layer	Maximum pooling, length of filter is 2, moving step of filter is 2
5 th	Full connection layer	<i>Dropout</i> [45] is added to avoid over-fitting phenomenon
6 th	Full connection layer	512 nodes

The Maximum Pooling is applied in 2nd and 4th hidden layers for two reasons.

- I. By eliminating non-maximal values, it reduces computation for upper layers.
- II. It provides a form of translation invariance.

Because the essential of this study is a regression problem, the output from 6th hidden layer will be the output from the whole CNN.

The activation function, *Rectified Linear Units Function* (ReLU), used in LeNet-5 can speed up the training process, and ReLU is calculated by

$$f(x) = \max(x, 0) \quad (12)$$

The loss function for this study is the *mean square error* (MSE).

$$MSE(y, y') = \frac{\sum_{i=1}^n (y_i - y_i')^2}{n} \quad (13)$$

In order to avoid the over-fitting problem, the *regularization* is added to the loss

function, it means that an indicator of CNN's complexity is added to the loss function. Assuming that the loss function is $J(\theta)$, CNN doesn't optimize $J(\theta)$, but optimize $J(\theta) + \lambda R(w)$, where $R(w)$ is the CNN's complexity, λ is the proportion of the complex loss to the total losses.

There are two ways to evaluate the complexity, one is *L1 regularization*, known as *Lasso Regularization*.

$$R(w) = \|w\|_1 = \sum_i |w_i| \quad (14)$$

Another is *L2 regularization*, known as *Weight Decay*.

$$R(w) = \|w\|_2^2 = \sum_i |w_i^2| \quad (15)$$

Firstly, when using L1 regularization, if an element of the weight vector is a positive number, the element becomes smaller, conversely, becomes larger. It means that the purpose of L1 regularization is making the weight vector change toward 0 and making the weights "sparser". Therefore, L1 regularization can achieve the function similar to the feature selection. Otherwise, L2 regularization cannot make the weights "sparser" because that when an element is small, such as 0.001, the square of the element is smaller and can be ignored, so the model will not change the element into 0. Secondly, the formula of L1 regularization cannot be derived while L2 regularization's can. Since the derivative of the loss function needs to be calculated during optimization, the optimization of L2 regularization's loss function is easier. After comprehensive analysis, both L1 regularization and L2 regularization are used in this study.

$$R(w) = \sum_i [\alpha |w_i| + (1 - \alpha) w_i^2] \quad (16)$$

where α is the proportion of L1 regularization to the total regularization. And the loss function is

$$total_losses = MSE(y, y') + \lambda R(w) \quad (17)$$

In the reverse propagation process, the loss function is used to update weights and biases.

$$w_i \leftarrow w_i + \Delta w_i \quad (18)$$

$$b \leftarrow b + \Delta b \quad (19)$$

where

$$\Delta w_i = \eta (y' - y) x_i \quad (20)$$

$$\Delta b = \eta (y' - y) \quad (21)$$

where w_i is the initial weight, b is the initial bias, y is the actual value, y' is the predicted value, and η is the learning rate.

Learning rate η determines the update rate of each parameter, it's usually designated at a constant. However, once η is too large, η might cause that the prediction swings on both sides of the optimal value and CNN can't converge. On the contrary, if η is too small, although the CNN can converge eventually, the training speed will be greatly reduced. Therefore, the η can't be too large, nor too small. Meanwhile, a more flexible method for learning rate's determination is employed -- *exponential decay method*, and its mathematical function is Eq. (22). As shown in Fig. 7, through this method, the CNN can obtain a larger learning rate so that it can be quickly trained initially, and then the CNN gradually reduces the learning rate to ensure that the model can converge to the optimal value at the end of the training.

$$\eta = \eta_0 \cdot \text{decay_rate}^{(\text{global_step}/\text{decay_step})} \quad (22)$$

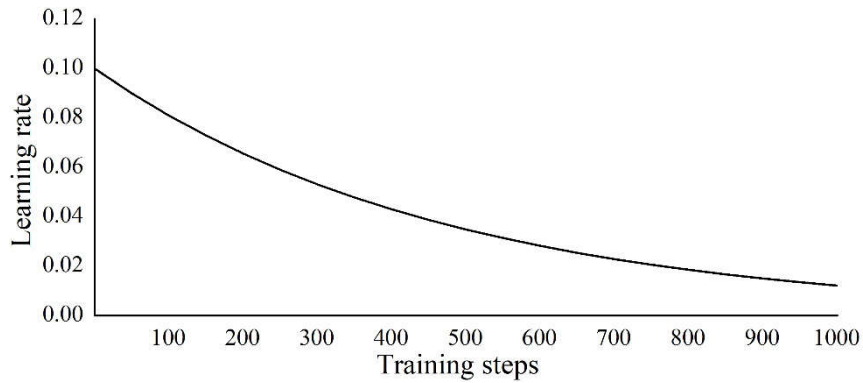


Fig. 7. Learning rate by exponential decay method.
(where η_0 is 0.1, decay_rate is 0.9, and decay_step is 50.)

As Hush and Horne [46] explained, network learning can be terminated under three different scenarios:

- I. When the MSE is less than the pre-designated value.

- II. When the pre-designated training steps is achieved.
- III. When a valid MSE sample has increased.

For the first two scenarios, it would easily over-fit for basing upon pre-designated value. Smith [47] suggested using cross-validation to prevent over-fitting. Therefore, the cross-validation rule is employed to this study.

4. Experiments and analysis

4.1. Test functions

This section illustrates the application of a NN to some typical high-dimensional and strong nonlinear mathematical models shown in Table 5. Subsequently, NN's capability is evaluated. For selecting mathematical models, we try to cover the operations including index, trigonometric function, absolute value, tired ride and accumulate to ensure we can achieve a comprehensive assessment of the NNs.

Table 5 Mathematical functions employed by this study.

Models' Name	Function	Description
Model1: Griewank	$f(x) = \sum_{i=1}^d \frac{x_i^2}{4000} - \prod_{i=1}^d \cos \frac{x_i}{\sqrt{i}} + 1$	Griewank function has many widespread local minima which are regularly distributed. The function is usually evaluated on the hypercube [-600, 600]
Model 2: Ackley	$f(x) = -20 \exp \left(-0.2 \sqrt{\frac{1}{d} \sum_{i=1}^d x_i^2} \right) - \exp \left(\frac{1}{d} \sum_{i=1}^d \cos 2\pi x_i \right) + 20 + \exp(1)$	Ackley function is widely used for testing optimization algorithms. The function is usually evaluated on the hypercube [-32.768, 32.768]
Model 3: Schwefel	$f(x) = 418.9829d - \sum_{i=1}^d x_i \sin \sqrt{ x_i }$	Schwefel function with many local minima is complex. The function is usually evaluated on the hypercube [-500, 500]
Model 4: Levy (Modified)	$f(x) = \sum_{i=1}^d \left\{ (x_i - 1)^2 \left[1 + \sin^2(3\pi x_i) \right] \right\}$	This function is usually evaluated on the hypercube [-10, 10]
Model 5: Sum of Different Powers	$f(x) = \sum_{i=1}^d x_i ^{i+1}$	This is unimodal and is usually evaluated on the hypercube [-1, 1]

Model 6: Rastrigin	$f(x) = 10d + \sum_{i=1}^d [x_i^2 - 10 \cos(2\pi x_i)]$	This has several local minima. It is highly multimodal, but locations of the minima are regularly distributed. The function is usually evaluated on the hypercube [-5.12, 5.12]
Model 7: Schaffer N2 (Modified)	$f(x) = 0.5 + \frac{\sin^2\left(\sum_{i=1}^d (-1)^i x_i^2\right) - 0.5}{\left[1 + 0.001 \sum_{i=1}^d x_i^2\right]^2}$	Schaffer function. This function is usually evaluated on the hypercube [-100, 100]
Model 8: Schaffer N4 (Modified)	$f(x) = 0.5 + \frac{\cos\left[\sin\left(\sum_{i=1}^d (-1)^i x_i^2\right)\right] - 0.5}{\left[1 + 0.001 \sum_{i=1}^d x_i^2\right]^2}$	Schaffer function. This function is usually evaluated on the hypercube [-100, 100]

4.2. Performance criteria

In this study, the performance of each NN is measured from accuracy and robustness. The accuracy is indicated by the model's predict ability during the design space. While the robustness is indicated by the high-precision acquisition capabilities during different problems.

For accuracy, the goodness-of-fit of training data is not enough to illustrate the model's accuracy. Therefore, additional testing samples are necessary for further verify the accuracy of the model trained by NN. In order to evaluate the training results comprehensively, several expressions of error in Table 6 [2, 3] are employed, where *STD* is standard deviation. The RMSE indicates the overall accurate approximation, while the MAE can reveal the presence of regional areas of poor approximation. The RAAE is usually related with MSE and a large RMAE indicates a though the RAAE may be great, so a small RMAE is preferred. However, because that the input interval and dimension from different NNs and situations are different, these statistics enable comparisons only within each NN.

Table 6 Criteria for error.

Name	Expression
Maximal Absolute Error (MAE)	$\max(y_i - y_i')$

Average Absolute Error (AAE)	$\sum_{i=1}^n y_i - y_i' / n$
Root Mean Square Error (RMSE)	$\sqrt{\sum_{i=1}^n (y_i - y_i')^2 / n}$
Relative Average Absolute Error (RAAE)	$\sum_{i=1}^n y_i' - y_i / (n \cdot STD)$
Relative Maximum Absolute Error (RMAE)	$\max(y_i' - y_i) / STD$

However, errors shown above cannot clearly present the difference between the actual value and the predict value of each testing sample, the χ_i is calculated by Eq. (23). In order to better display and compare the testing sample's χ_i s including maximum value and minimum value under different situations, testing points are re-ordered and displayed according to the levels of their χ_i s.

$$\chi_i = 1 - \left| \frac{y_i' - y_i}{y_i} \right| = 1 - RE \quad (23)$$

The robustness of NN is indicated by the variance between its χ_i [2] and is calculated by Eq. 24. A small σ^2 means a good performance in robustness, on the contrary, a big σ^2 means bad.

$$\sigma^2 = \frac{\sum (\chi_i - \mu)^2}{n} \quad (24)$$

where μ is the average of χ_i .

4.3. Distribution of samples

As is known to all, with the increase of dimension and expand of interval, the number of necessary training samples increases rapidly. It is necessary to know the most reasonable number of training samples once the interval, dimension and the maximum RE are determined, in order to avoid the wasting time of redundant training samples. By comparing the results for training different sample's sizes under a same NN, we select the minimum training samples which meets the requirement of the NN's training.

4.4. Result and discussion

As mentioned above, the closer the χ_i to 1 is, the higher precision the model is. For both RAAE and RMAE, a smaller value indicates a higher accuracy. And for variance, a

smaller value indicates a stronger robustness.

4.4.1. Performance for different input intervals. As shown in Fig. 8, the errors and variances of Griewank function show the robustness for different input intervals by the BPNN when the input dimension is 2D. As shown in Fig. 9, only very few sample's χ_i s are less than 60% when each x_i belongs to $[0, 50]$. And more than 80% sample's χ_i s in all intervals are more than 80%.

It is noted that BPNN performs satisfactory in terms of both accuracy and robustness for a high-order nonlinear and low-dimensional problem. However, the robustness, although small for BPNN, becomes larger when the interval expands.

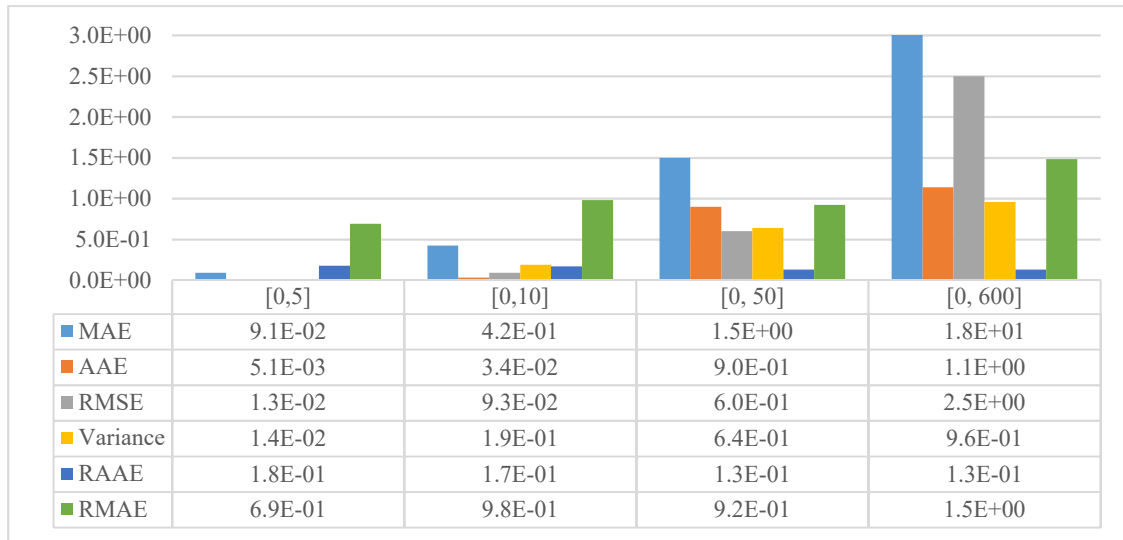


Fig. 8. Comparison of errors and variances of testing samples between different intervals when the input dimension is 2 by BPNN.

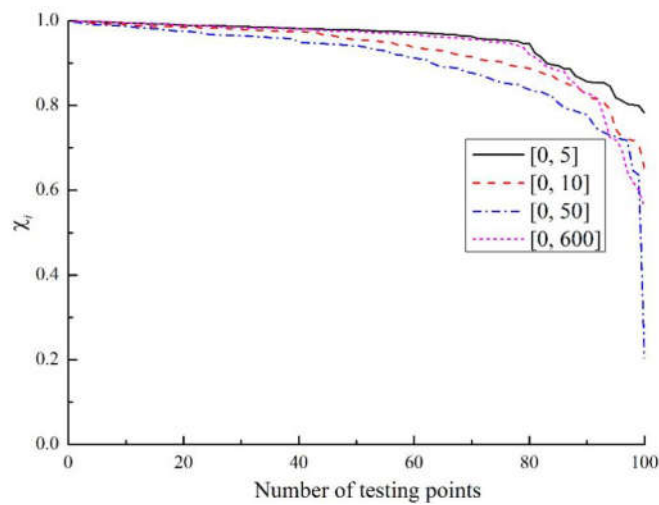


Fig. 9. Comparison of testing sample's χ_i s between different intervals when the input dimension is 2 by BPNN.

For CNNs, as shown in Figs. 10 and 11, the changes of error, variance and χ_i with the increase of input dimension are presented when modeling the Griewank function. It is found that with expand of the interval, the variance is still very small and χ_i s from all intervals are more than 80%. It indicates that CNN's robustness and calculation ability are excellent when analyzing high-dimensional and strong nonlinear problems.

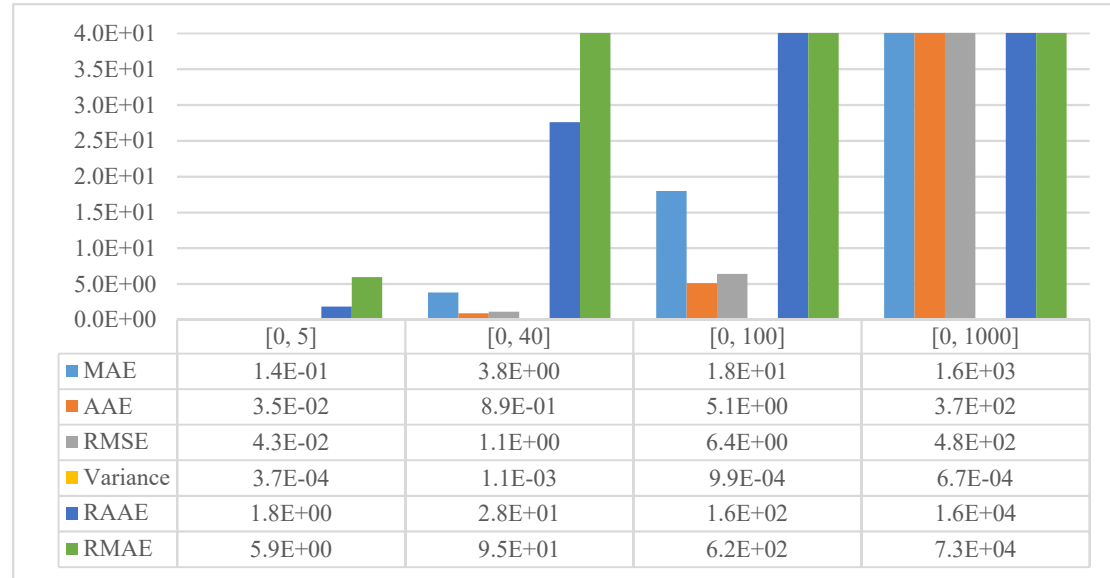


Fig. 10. Comparison of errors and variances of testing samples between different intervals when the input dimension is 144 by CNN.

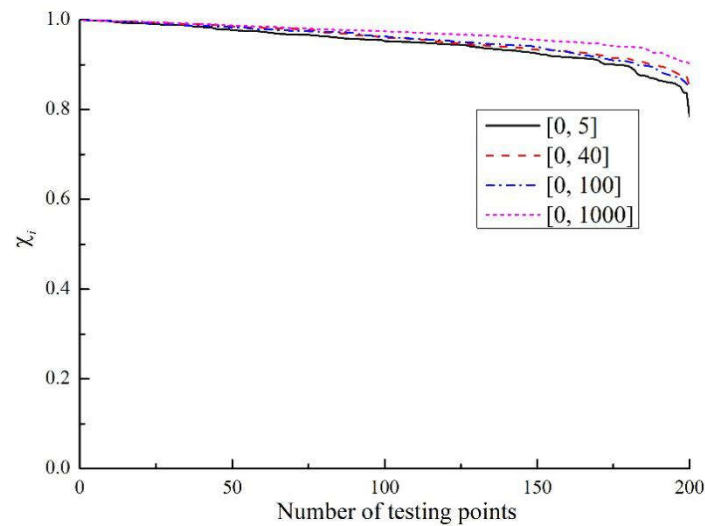


Fig. 11. Comparison of testing sample's χ_i s between different intervals when the input dimension is 144 by CNN.

Overall, in terms of the accuracy and robustness, with the increase of input intervals, CNN is proved to be the best choice compared to the commonly used BPNN when

handling high-dimensional and strong nonlinear problems.

4.4.2. Performance for different input dimensions. As shown in Figs. 12 and 13, the errors, variance and χ_i s of the Griewank function are presented for different dimensions by BPNN when the input variables are in $[0, 100]$. The variance rapidly increases and more than 40% testing sample's χ_i s are less than 80%. Even when the dimension is 10 or 20, some χ_i s are negative. It indicated that the BPNN performs powerless in robustness and accuracy. And it is noted that the dimension which the BPNN can model is 20 at most. And with the increase of input dimension, BPNN's robustness trends toward sharp decline. Therefore, with the increase of input dimension, BPNN performs powerless.

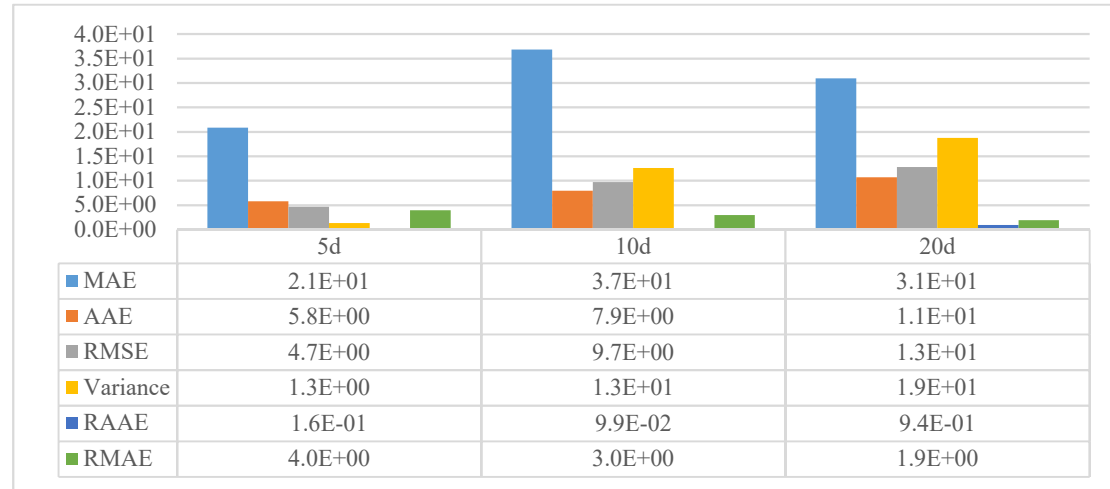


Fig. 12. Comparison of errors and variance of testing samples between different dimensions when the interval is $[0, 100]$ by BPNN.

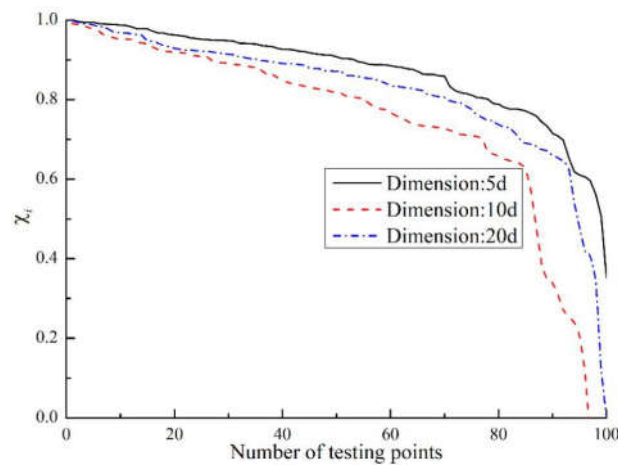


Fig. 13. Comparison of testing sample's χ_i s between different dimensions when the interval is $[0, 100]$ by BPNN.

As shown in Figs. 14 and 15, the training results of the Griewank function by CNN are presented when the interval is $[0, 1000]$. From the Fig. 15, almost all testing sample's χ_i s are more than 90%, and it is amazing that the variances are less than 10^{-3} . Thus, the calculation ability and robustness of CNN are very surprised to us when analyzing a high-dimensional and strong nonlinear problem.

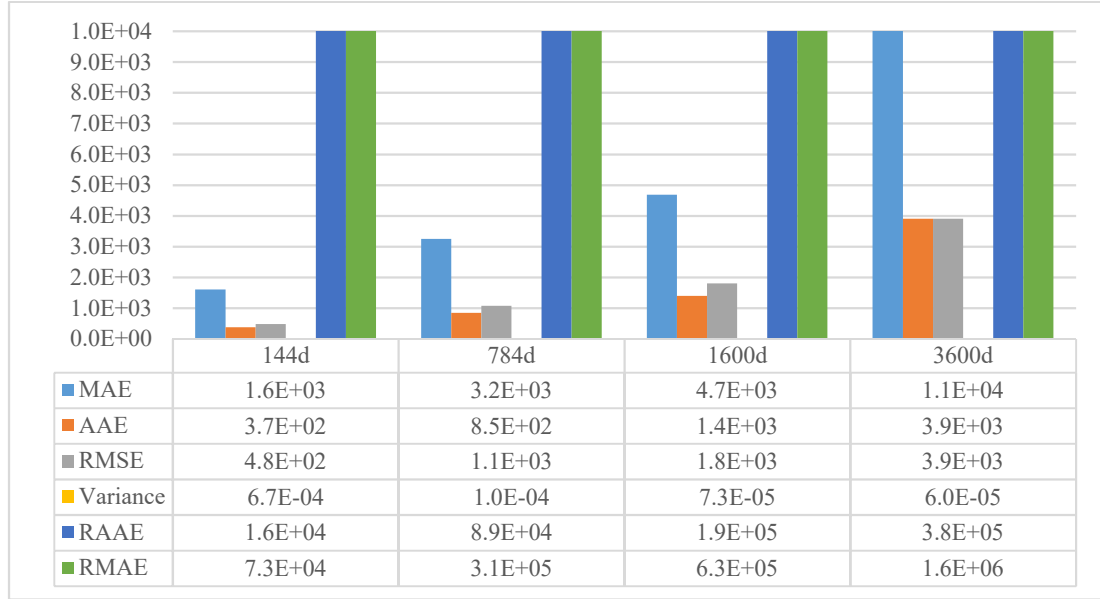


Fig. 14. Comparison of errors and variance of testing samples between different dimensions when the interval is $[0, 1000]$ by CNN.

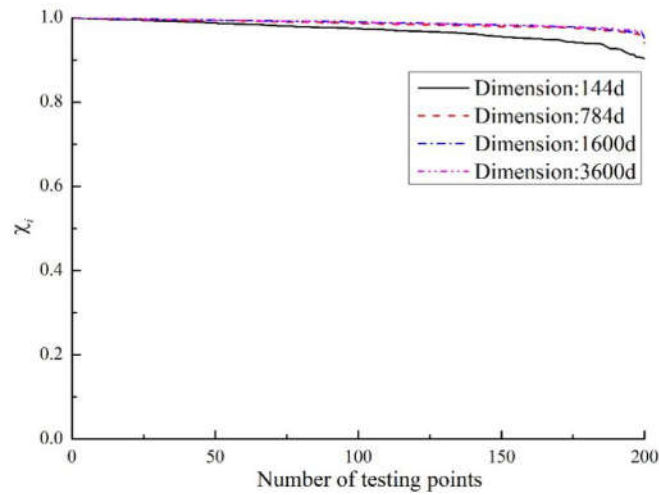


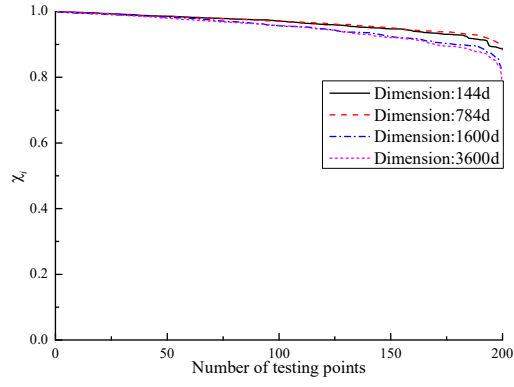
Fig. 15. Comparison of testing sample's χ_i s between different dimensions when the interval is $[0, 1000]$ by CNN.

4.4.3. Performance for modeling other mathematical models. To further judge the CNNs' ability, some other mathematical models shown in Table 5 are calculated.

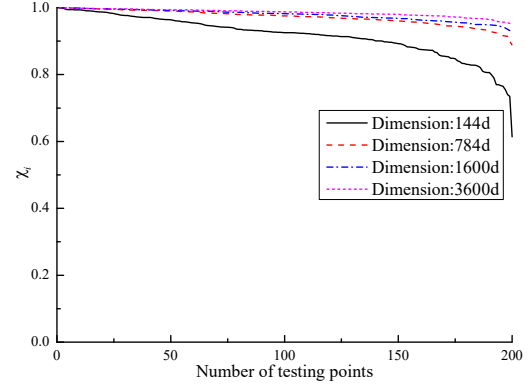
Moreover, Table 7 shows the errors and variances and Fig. 16 presents the χ_i s. The interval is [-100, 100] for Ackley function, [-1000, 1000] for Schwefel function, [-10, 10] for Levy function, [-1, 1] for Sum of Different Powers function, [-10, 10] for Rastrigin function, [-100, 100] for Schaffer N2 function and [-100, 100] for Schaffer N4 function. The column of variance whose values are generally less than 10^{-2} in Table 7 can further illustrate the performance of CNN's robustness. As shown in Fig. 16, although the χ_i 's interval of the Sum of Different Powers function, Schaffer N2 function and Schaffer N4 function are a little worse than other functions', the results calculated by CNN are very satisfactory compared with existing methods.

Table 7 Variances and errors between different functions by CNN.

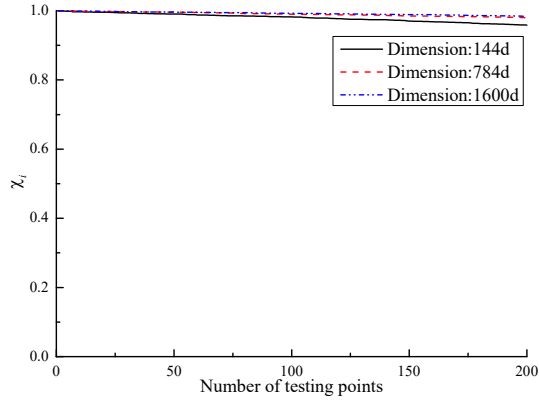
Function	Dimension	Variance	MAE	AAE	RMSE	RAAE	RAME
Ackley	144D	7.2×10^{-4}	2.4×10^0	7.7×10^{-1}	9.7×10^{-1}	3.1×10^1	8.3×10^1
	784D	5.5×10^{-4}	2.5×10^0	7.3×10^{-1}	8.9×10^{-1}	2.9×10^1	1.2×10^2
	1600D	1.3×10^{-3}	3.8×10^0	1.1×10^{-1}	1.3×10^0	2.8×10^1	1.3×10^2
	3600D	1.6×10^{-3}	4.9×10^0	1.3×10^0	1.4×10^0	5.0×10^1	3.6×10^2
Schwefel	144D	3.7×10^{-3}	1.8×10^0	4.9×10^3	6.0×10^3	8.1×10^4	3.0×10^5
	784D	4.7×10^{-4}	4.1×10^0	9.4×10^3	1.2×10^4	4.3×10^5	1.8×10^6
	1600D	2.6×10^{-4}	5.5×10^0	1.5×10^4	1.9×10^4	9.0×10^5	8.3×10^6
	3600D	1.1×10^{-4}	7.2×10^0	2.2×10^4	2.7×10^4	2.0×10^6	6.5×10^6
Levy	144D	8.0×10^{-4}	9.9×10^0	3.3×10^4	3.8×10^4	8.7×10^5	3.5×10^6
	784D	1.4×10^{-4}	2.4×10^5	9.6×10^4	9.9×10^4	5.3×10^6	2.0×10^7
	1600D	9.2×10^{-5}	4.1×10^5	1.5×10^5	1.5×10^5	1.0×10^7	4.3×10^7
Sum of Different Powers	144D	3.1×10^{-2}	3.8×10^0	9.9×10^{-1}	1.2×10^0	5.5×10^0	2.2×10^1
	784D	5.1×10^{-2}	5.3×10^0	1.4×10^0	1.8×10^0	6.3×10^0	2.4×10^1
	1600D	2.9×10^{-2}	6.3×10^0	1.5×10^0	1.5×10^0	9.2×10^0	3.7×10^1
	3600D	5.3×10^{-2}	6.9×10^0	1.8×10^0	2.2×10^0	8.0×10^0	3.0×10^1
Rastrigin	144D	4.5×10^{-4}	2.9×10^2	7.6×10^1	9.4×10^1	3.5×10^3	1.4×10^4
	784D	5.2×10^{-5}	1.2×10^3	3.1×10^2	3.9×10^2	4.2×10^4	1.6×10^5
	1600D	3.4×10^{-5}	2.0×10^3	5.6×10^2	7.0×10^2	9.6×10^4	3.4×10^5
	3600D	3.4×10^{-6}	4.4×10^3	2.2×10^3	2.3×10^3	3.7×10^5	7.4×10^5
Schaffer N2	144D	1.8×10^{-2}	6.7×10^{-1}	5.1×10^{-2}	8.4×10^{-2}	3.9×10^{-1}	5.1×10^0
	784D	1.6×10^{-2}	7.5×10^{-1}	6.4×10^{-2}	9.0×10^{-2}	5.0×10^{-1}	5.9×10^0
	1600D	1.7×10^{-2}	4.6×10^{-1}	6.2×10^{-2}	9.0×10^{-2}	4.7×10^{-1}	3.5×10^0
	3600D	1.0×10^{-2}	2.3×10^{-1}	7.2×10^{-2}	8.8×10^{-2}	7.1×10^{-1}	2.3×10^0
Schaffer N4	144D	1.5×10^{-2}	6.5×10^{-1}	1.1×10^{-1}	1.2×10^{-1}	3.6×10^{-1}	5.3×10^0
	784D	6.5×10^{-3}	5.2×10^{-1}	1.3×10^{-1}	1.0×10^{-1}	6.3×10^{-1}	6.4×10^0
	1600D	6.2×10^{-3}	2.0×10^{-1}	1.4×10^{-1}	1.1×10^{-1}	7.0×10^{-1}	2.4×10^0



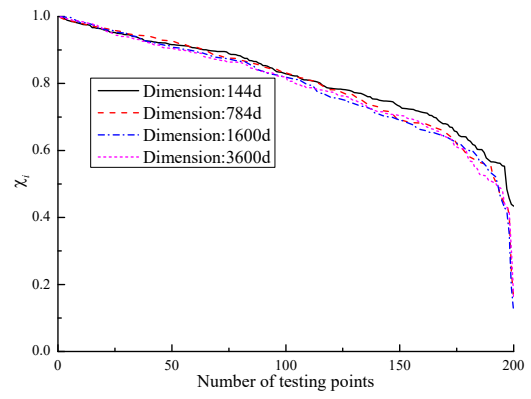
(a) Ackley function



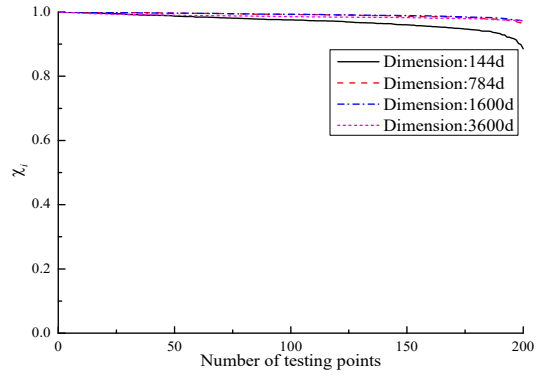
(b) Schwefel function



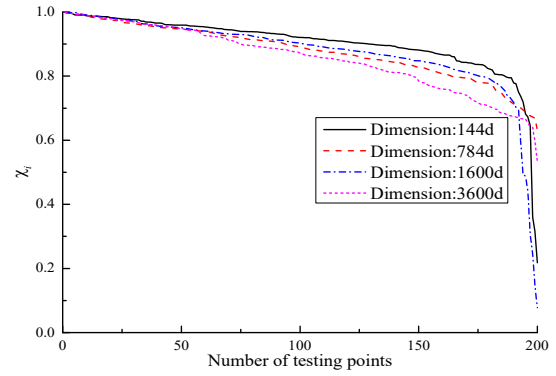
(c) Levy function



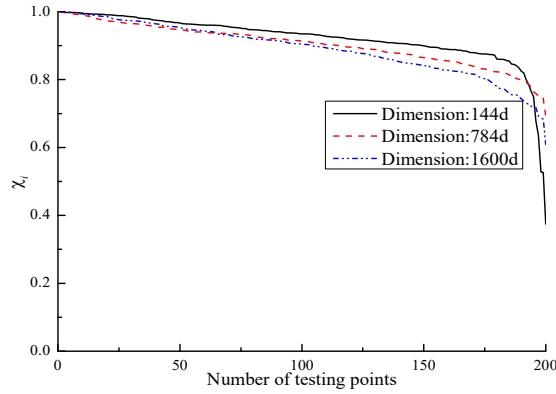
(d) Sum of Different Powers function



(e) Rastrigin function



(f) Schaffer N2 function



(g) Schaffer N4 function

Fig. 16. Model's χ_i s under different dimensions by CNN.

We also observe another interesting law about CNN, when the dimension is low, the accuracy and robustness are generally worse than those of a higher dimension. This rule further confirms the absolute advantage of CNN's capability in high-dimensional problems.

4.4.4. Performance under different sample sizes. We end our analysis with a comparison of training different sizes of training samples. The training results by BPNN are presented in Fig. 17, the interval is $[0, 100]$ and dimension is 2, it can be seen that there is a clear decline when the training sample's size is less than 3000. Therefore, under the current parameters, BPNN's minimum training sample's size should be beyond 3000. As shown in Figs. 18- 25, the results calculated by the CNN indicate that only 2000 necessary training samples can CNN get the results with high accuracy. Moreover, we also find that BPNNs gradually converge after 20000 training steps, and CNNs only need 3000 training steps to get a convergence result. So the efficiency of CNN is better.

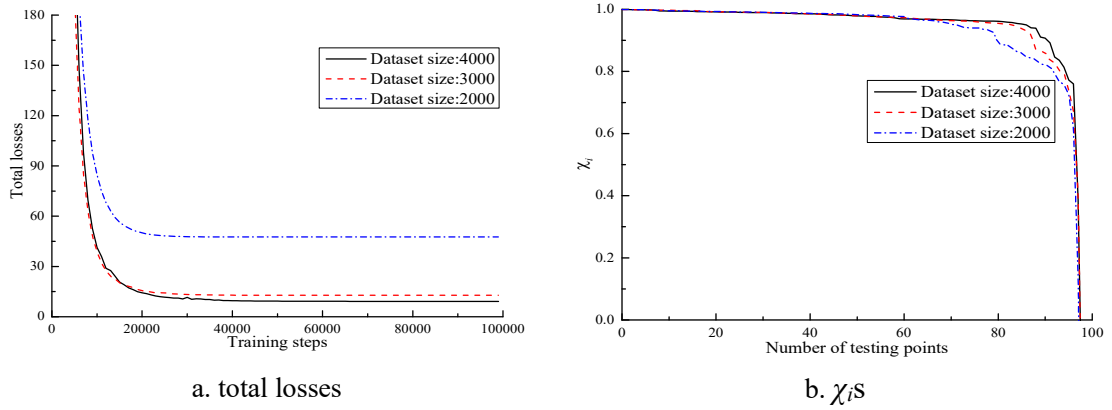


Fig. 17. Training results of Griewank function under different dataset sizes by BPNN when the interval is $[0, 100]$ and dimension is 2.

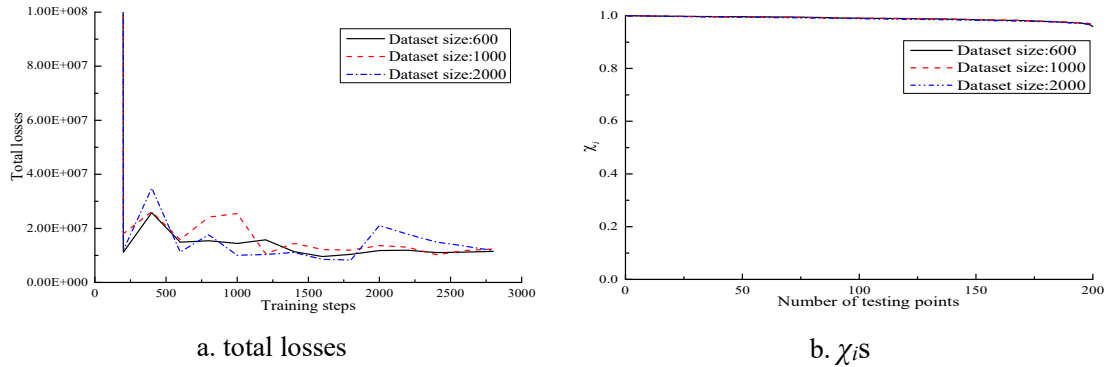


Fig. 18. Training results of Griewank function under different dataset sizes by CNN when the interval is $[0, 1000]$ and dimension is 3600.

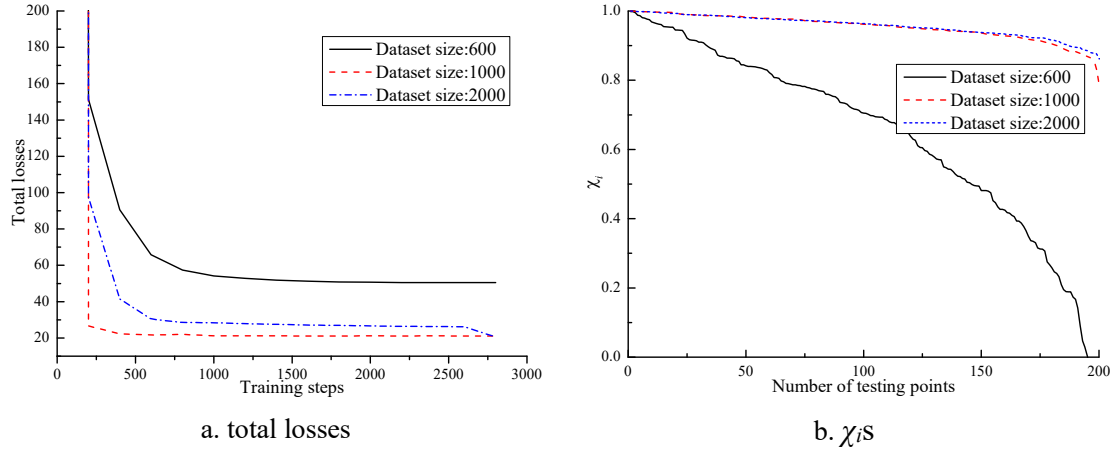


Fig. 19. Training results of Ackley function under different dataset sizes by CNN when the interval is $[-1000, 1000]$ and dimension is 3600.

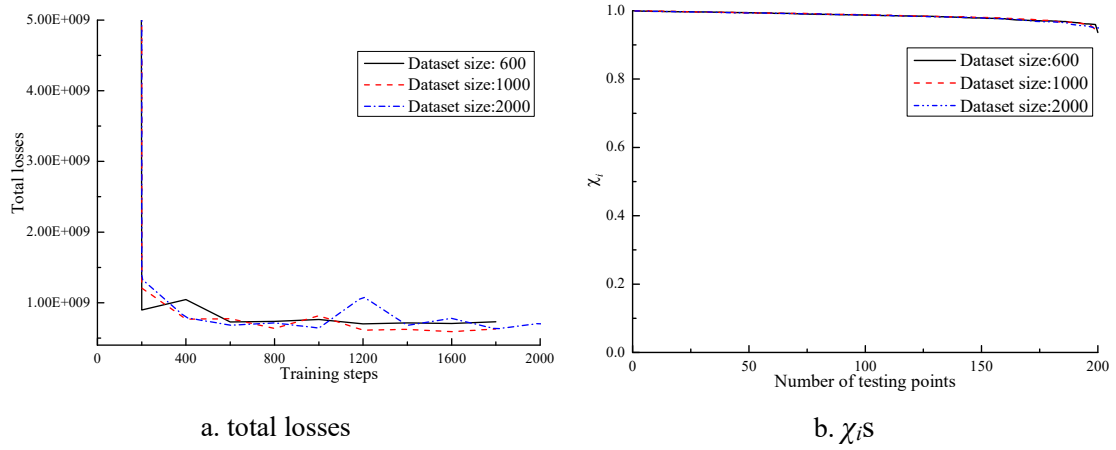


Fig. 20. Training results of Schwefel function under different dataset sizes by CNN when the interval is $[-500, 500]$ and dimension is 3600.

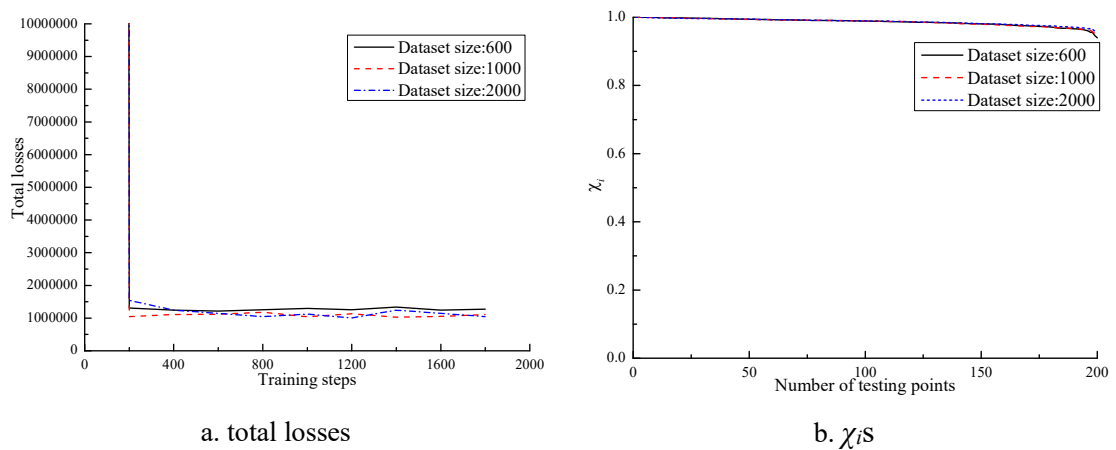


Fig. 21. Training results of Levy function under different dataset sizes by CNN when the interval is $[-10, 10]$ and dimension is 1600.

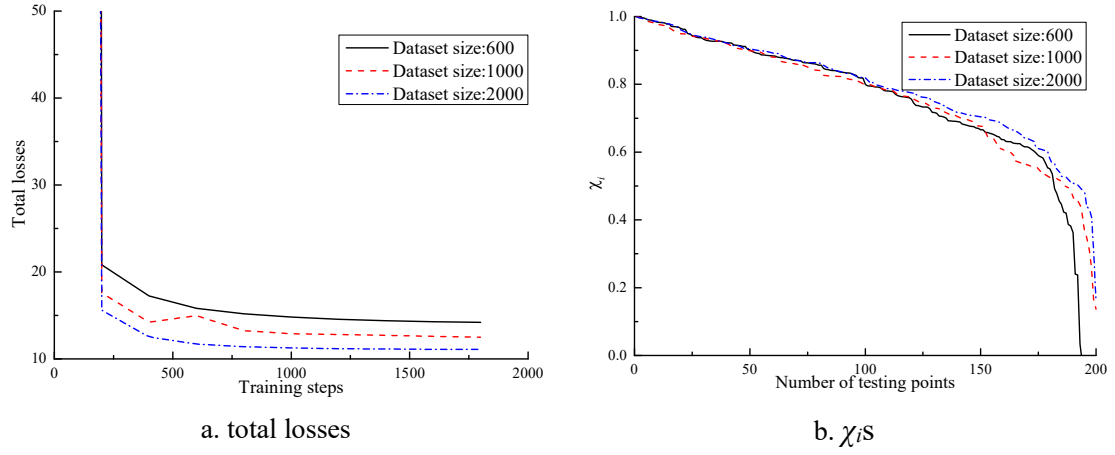


Fig. 22. Training results of Sum of Different Powers function under different dataset sizes by CNN when the interval is $[-1, 1]$ and dimension is 3600.

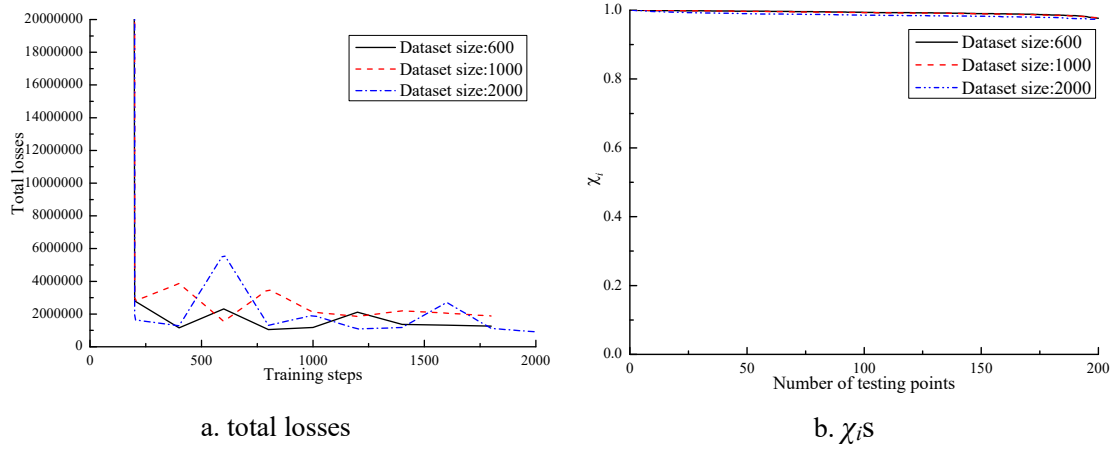


Fig. 23. Training results of Rastrigin function under different dataset sizes by CNN when the interval is $[-10, 10]$ and dimension is 3600.

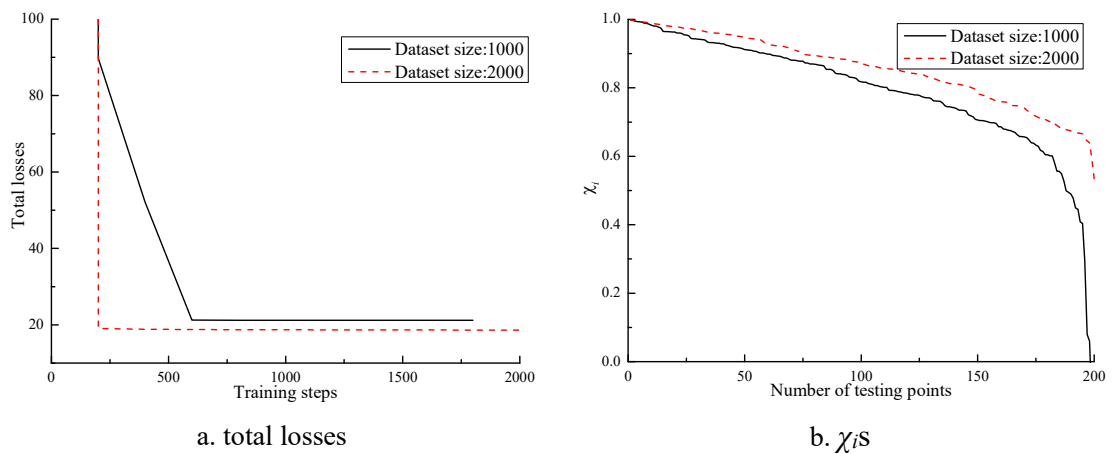


Fig. 24. Training results of Schaffer N2 function under different dataset sizes by CNN when the interval is $[-100, 100]$ and dimension is 3600.

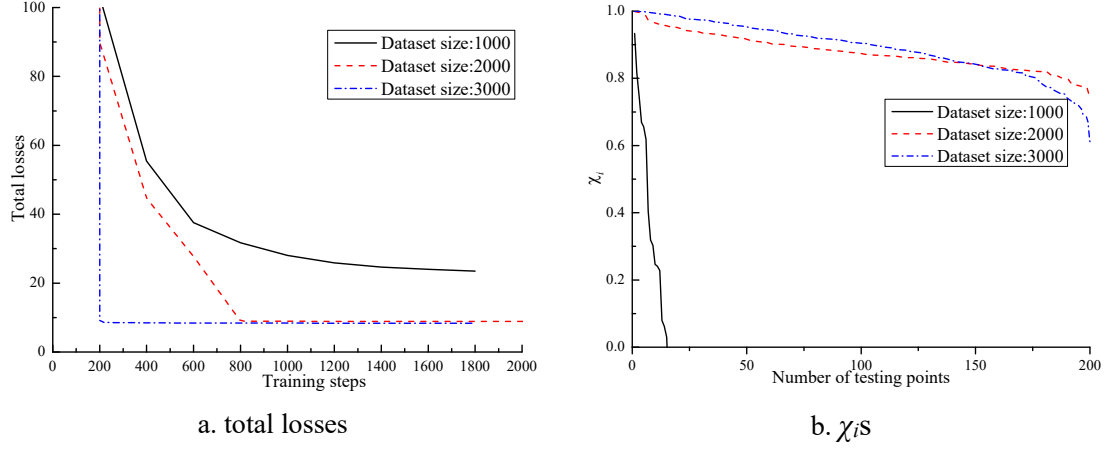


Fig. 25. Training results of Schaffer N4 function under different dataset sizes by CNN when the interval is $[-100, 100]$ and dimension is 1600.

5. Complex geometric modeling by CNN

It is well known that the CNN can handle many problems. While in our views, on geometric issues, the CNN has its unique advantages.

Isogeometric analysis [48-51] (IGA) is a popular method of numerical solution of the physical field recent years. The main advantage of IGA based on Non-uniform Rational B-splines (NURBS) is the integration of Computer Aided Design (CAD) and Computer Aided Engineering (CAE). Moreover, IGA can provide a new method that can combine design, analysis and optimization. Non-uniform Rational B-splines (NURBSs) are a standard basis function used in CAD and CG, and the most preferred computational technology in IGA. Recent applications [52-55] of IGA include solids, structures, fluids, and fluid–structure interaction. It is known that NURBSs are built from B-splines through a projective transformation [56] and inherit their superior approximation power, and are constructed by lots of control points and knot vectors whose modification provides a feasible way to optimization. In the IGA and the NURBS-enhanced FEA, where NURBS is adopted as the basis function, the numerical quadrature needs more and more computational load with the increase of the model's scale, and then researches for faster quadrature rules have been very active [57-61]. And this issue is more obvious in the structural optimization problems. Due to the limitations of computers' computational ability, we cannot solve issues of large design variables using the IGA. The method in this study utilizes CNN to extract rules inherent in an IGA application,

which usually are implicit and sometimes too complicated to grasp from the large amount of available data to solve the problem that IGA's design variables cannot be too many.

In this study, Rhinoceros software is applied to provide the input information of a tubular structure shown in Fig. 26. Subsequently, NURBS is constructed and applied to geometry model and analysis model. As shown in Figs. 27(b) and (c), the Degrees of Freedom (DOFs) on bottom surface marked in red are fixed, and as shown in Fig. 27(a), three concentrated forces which are equal to $3 \times 10^5 N$ in y direction are enforced to the control points marked in orange. Finally, the stress of the structure is analyzed by IGA. The initial control points and the weight factors are used as the input variables of the model, and the set of maximum stress after 2500 iterations is used as the output information. By modifying the values of input variables, 2000 results as training samples and 500 results as testing samples are calculated for CNN.

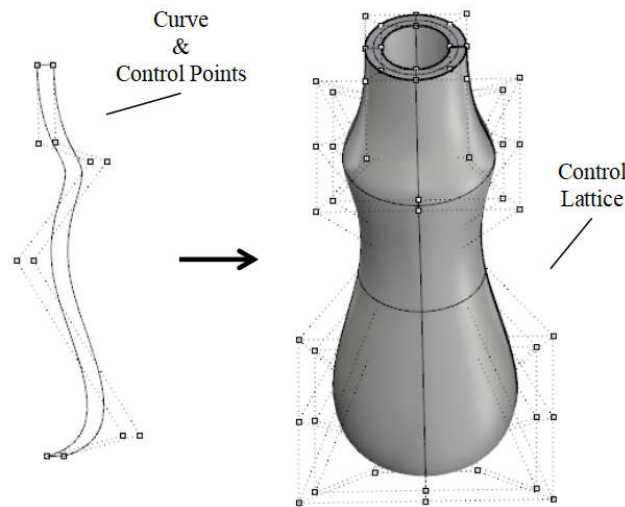


Fig. 26. The control lattice for the tubular structure.

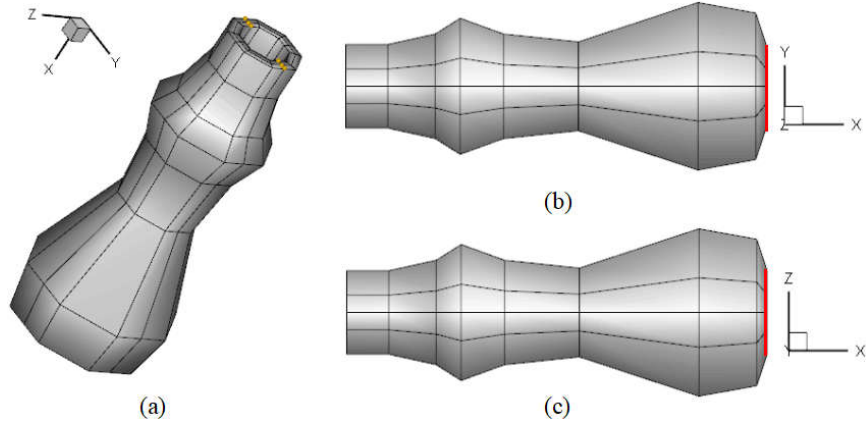


Fig. 27. Constraints and load of the tubular structure.

For each sample, design variables include 324 control points, and each control point includes cylindrical coordinate (r, φ, z) which calculates by Eq. 25 and a weight factor w , so the input dimension is $324 \times (3+1) = 1296$, the output is the maximum stress of the tubular structure. As shown in Figs. 28 and 29, the results by CNN are presented, it can be seen that the errors, variance and χ_i s are surprised to us.

$$\begin{cases} x = r \cos \varphi \\ y = r \sin \varphi \\ z = z \end{cases} \quad (25)$$

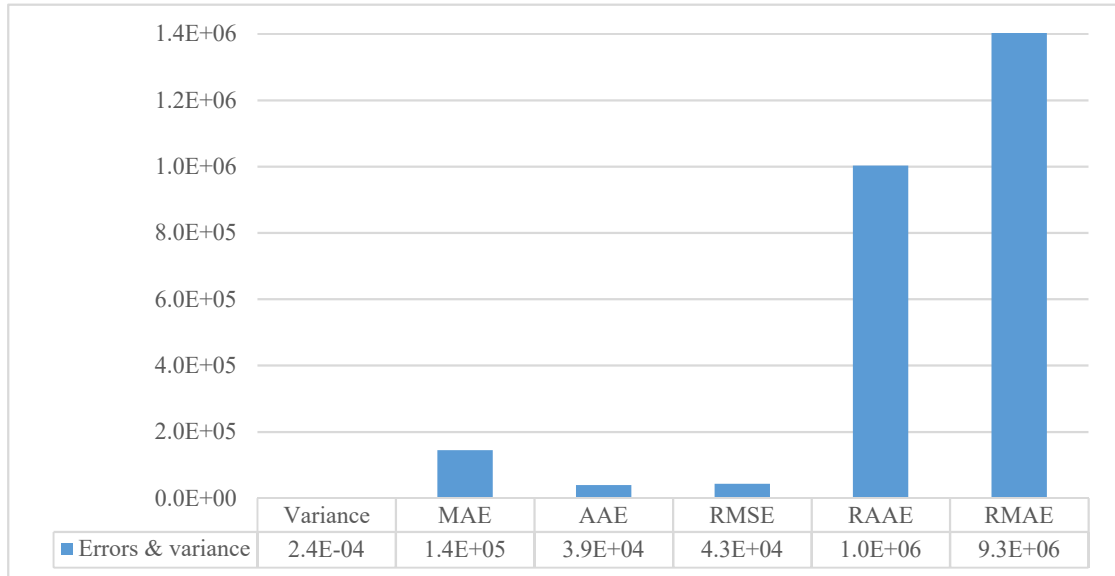


Fig. 28. Errors and variance of testing samples.

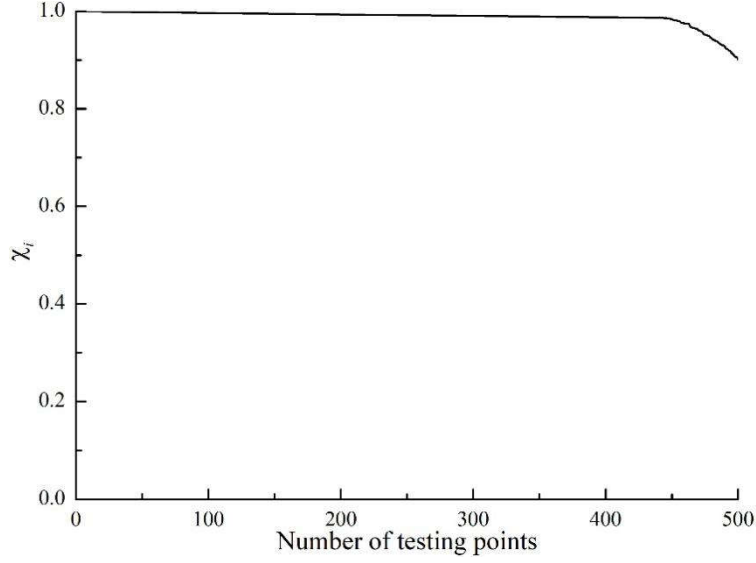


Fig. 29. Testing sample's χ_i s.

Then the CNN model is optimized using genetic algorithm (GA) reanalysis methods. The tubular structure is optimized by changing the coordinate of the control points. And the objective function to be minimized is the stress of the tubular structure. The shape of tubular structure is chosen as the design variable. In particular, the tubular structure changes only in the direction of the r axis. Therefore, the optimization problem is stated as

$$\min y = CNN(\mathbf{B}(\Delta r_1, \Delta r_2, \dots, \Delta r_{324})) \quad (26)$$

s.t.

$$\Delta r_i \in [0.5, 2.5] \quad (27)$$

where CNN is the maximal stress of the tubular structure, \mathbf{B} is the control points which is set as design variables, and Δr_i is the amplification factors of control points. The optimized shape and corresponding stress analysis results are shown in Fig. 30. It can be found that only 2000 training samples from the IGA can CNN get a very satisfactory model, and CNN model can combine the reanalysis methods to further improve the efficiency of optimization. This section further illustrates the application of CNN to high dimensional problems.

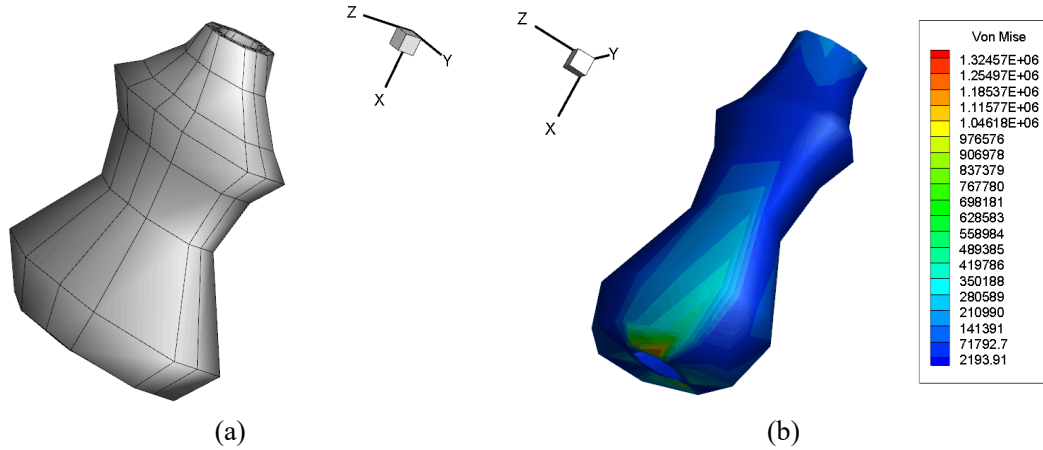


Fig. 30. The optimized shape and stress analysis results of the tubular structure.

Conclusions

In conclusion, this study focuses on the rule extraction capability of CNN, showing the possibility of its new application to the high dimensional and strong nonlinear problems in which existing methods have never been successful

In this study, we investigate convolutional neural networks (CNNs) as alternative technique for high-dimension and strong nonlinear problems using limited training samples. The computationally efficient theory behind CNN is reviewed, and CNN approximations are compared against the aforementioned BPNN using several complex mathematical functions. CNN achieves more accurate and more robust function approximations than the BPNN, and shows great potential for modeling applications.

In terms of the accuracy and robustness, can provide the observations and conclusions from Section 4 as follows. CNN excels in majority mathematical models. In terms of the input interval and dimension, accuracy and robustness of CNN are far superior to other methods. For the most difficult problems, i.e. high-dimensional and strong nonlinear problems, we compared the ability between CNN and BPNN, the training results represent that CNN can construct extremely high-precision models with limited samples. While BPNN requires a large number of samples, and its result is not satisfactory. From the above observations, we can conclude that CNN is the most dependable model for highly nonlinear and dimensional problems.

Finally, an application of CNN to optimization of complex geometric structure is also proposed. CNN, which is based on the characteristics of location connection, weight

sharing and local pooling has overstepped the limits of the present popular metamodeling techniques, widening its application scope to a large extent.

Acknowledgments

This work has been supported by Project of the Key Program of National Natural Science Foundation of China under the Grant Numbers 11572120, 11302266 and 61232014.

References

- [1] Oron G. Statistical tools for simulation practitioners : Jack P.C. Kleijnen Volume 76 in: Statistics: Textbooks and Monographs, Marcel Dekker, New York, 1987, 448 pages, \$69.75. European Journal of Operational Research. 1988;34(2):240-1.
- [2] Jin R, Chen W, Simpson TW. Comparative studies of metamodelling techniques under multiple modelling criteria. Structural & Multidisciplinary Optimization. 2000;23(1):1-13.
- [3] Clarke SM, Griebisch JH, Simpson TW, editors. Analysis of Support Vector Regression for Approximation of Complex Engineering Analyses. ASME 2003 International Design Engineering Technical Conferences and Computers and Information in Engineering Conference; 2005.
- [4] Hinton A, Kwiatkowska M, Norman G, Parker D, editors. PRISM: A Tool for Automatic Verification of Probabilistic Systems. International Conference on Tools and Algorithms for the Construction and Analysis of Systems; 2006.
- [5] Lin CT, Lee CSG. Neural-Network-Based Fuzzy Logic Control and Decision System. IEEE Transactions on Computers. 1991;40(12):1320-36.
- [6] Sanger TD. Optimal unsupervised learning in a single-layer linear feedforward neural network. Neural Networks. 1989;2(6):459-73.
- [7] Venkat V, Chan K. A neural network methodology for process fault diagnosis. Aiche Journal. 2010;35(12):1993-2002.
- [8] Qian L, Winfree E, Bruck J. Neural network computation with DNA strand displacement cascades. Nature. 2011;475(7356):368-72.

- [9] Tsai CC, Huang HC, Lin SC. Adaptive Neural Network Control of a Self-Balancing Two-Wheeled Scooter. *IEEE Transactions on Industrial Electronics*. 2010;57(4):1420-8.
- [10] Sudheer KP, Gosain AK, Ramasastri KS. A data-driven algorithm for constructing artificial neural network rainfall-runoff models. *Hydrological Processes*. 2010;16(6):1325-30.
- [11] Liu C, Shu T, Chen S, Wang S, Lai KK, Gan L. An improved grey neural network model for predicting transportation disruptions. *Expert Systems with Applications*. 2016;45(C):331-40.
- [12] Yang Z, Liu HC, Amp TE. A Sweeping Robot Path Pathfinding Algorithm Based on Bp Neural Network. *Computer Knowledge & Technology*. 2017.
- [13] Williams RJ, Zipser D. A Learning Algorithm for Continually Running Fully Recurrent Neural Networks. *Neural Computation*. 2014;1(2):270-80.
- [14] Zheng XJ, Zhang GZ, Xie ZY. Research on a High-Precision Algorithm of RBF Neural Network and Its Applications. *Journal of Northeastern University*. 2009;30(9):1314-7+45.
- [15] Krishnan V, Ulrich KT. Product Development Decisions: A Review of the Literature. *Management Science*. 2001;47(1):1-21.
- [16] Bing W. A Classification Method for Large Data Sets Based on the Changing Width Factor RBF Networks. *Microelectronics & Computer*. 2015;32(6).
- [17] Liu J, Zhao H, Zhou R, Wang P. Exploration of High-Precision Adaptive Wavelet Neural Network Artificial Intelligence Method. *Journal of Frontiers of Computer Science and Technology*. 2016;10(8):1122-32.
- [18] Khaw JFC, Lim BS, Lim LEN. Optimal design of neural networks using the Taguchi method. *Neurocomputing*. 1995;7(3):225-45.
- [19] Kim YH. Study on Impact Mechanism for Beef Cattle Farming and Importance of Evaluating Agricultural Information in Korea Using DEMATEL, PCA and AHP. *Agricultural Information Research*. 2006;15(3):267-79.
- [20] Kaastra I, Boyd M. Designing a neural network for forecasting financial and economic time series. *Neurocomputing*. 1996;10(3):215-36.

- [21] Karsoliya S. Approximating Number of Hidden layer neurons in Multiple Hidden Layer BPNN Architecture. *International Journal of Engineering Trends & Technology*. 2012;3(6).
- [22] Rumelhart DE, editor McClelland and the PDP Research Group. *Symposium on Parallel and Distributed Processing*; 1986.
- [23] Rumelhart DE, Hinton GE, Williams RJ. Learning representations by back-propagating errors. *Nature*. 1986;323(6088):533-6.
- [24] Lecun Y, Bengio Y, Hinton G. Deep learning. *Nature*. 2015;521(7553):436-44.
- [25] Hu HY, Lee YC, Yen TM, Tsai CH. Using BPNN and DEMATEL to modify importance–performance analysis model – A study of the computer industry. *Expert Systems with Applications*. 2009;36(6):9969-79.
- [26] Boger Z, Guterman H, editors. *Knowledge extraction from artificial neural network models. IEEE International Conference on Systems, Man, and Cybernetics, 1997 Computational Cybernetics and Simulation*; 1997.
- [27] Han J, editor *Data mining techniques. ACM SIGMOD International Conference on Management of Data, Montreal, Quebec, Canada, June*; 1996.
- [28] Blum. *Neural Networks in C++*. NY:wiley. 1992.
- [29] Cun YL, Boser B, Denker JS, Howard RE, Hubbard W, Jackel LD, et al., editors. *Handwritten digit recognition with a back-propagation network. Advances in Neural Information Processing Systems*; 1990.
- [30] Krizhevsky A, Sutskever I, Hinton GE, editors. *ImageNet classification with deep convolutional neural networks. International Conference on Neural Information Processing Systems*; 2012.
- [31] Shen Y, He X, Gao J, Deng L, editors. *Learning semantic representations using convolutional neural networks for web search. Companion Publication of the International Conference on World Wide Web Companion*; 2014.
- [32] Grefenstette E, Blunsom P, Freitas ND, Hermann KM. A Deep Architecture for Semantic Parsing. *Computer Science*. 2014;30(5):1-15.
- [33] Kalchbrenner N, Grefenstette E, Blunsom P. A Convolutional Neural Network for Modelling Sentences. *Eprint Arxiv*. 2014;1.

- [34] Kim Y. Convolutional Neural Networks for Sentence Classification. Eprint Arxiv. 2014.
- [35] Wallach I, Dzamba M, Heifets A. AtomNet: A Deep Convolutional Neural Network for Bioactivity Prediction in Structure-based Drug Discovery. *Mathematische Zeitschrift*. 2015;47(1):34-46.
- [36] Liu Y, Racah E, Prabhat, Correa J, Khosrowshahi A, Lavers D, et al. Application of Deep Convolutional Neural Networks for Detecting Extreme Weather in Climate Datasets. 2016.
- [37] Clark C, Storkey A. Teaching Deep Convolutional Neural Networks to Play Go. Eprint Arxiv. 2015:1766-74.
- [38] Krizhevsky A. Learning Multiple Layers of Features from Tiny Images. 2009.
- [39] Roth HR, Lu L, Liu J, Yao J, Seff A, Cherry K, et al. Improving Computer-Aided Detection Using Convolutional Neural Networks and Random View Aggregation. *IEEE Transactions on Medical Imaging*. 2016;35(5):1170.
- [40] Szegedy C, Liu W, Jia Y, Sermanet P, Reed S, Anguelov D, et al., editors. Going deeper with convolutions. *Computer Vision and Pattern Recognition*; 2015.
- [41] Cireşan DC, Giusti A, Gambardella LM, Schmidhuber J, editors. Mitosis detection in breast cancer histology images with deep neural networks 2013.
- [42] Lecun Y, Bottou L, Bengio Y, Haffner P, editors. *Gradient-Based Learning Applied to Document Recognition*. IEEE; 1998.
- [43] Saxe AM, Pang WK, Chen Z, Bhand M, Suresh B, Ng AY, editors. On random weights and unsupervised feature learning. *International Conference on International Conference on Machine Learning*; 2012.
- [44] Lécun Y, Bottou L, Bengio Y, Haffner P. Gradient-based learning applied to document recognition. *Proceedings of the IEEE*. 1998;86(11):2278-324.
- [45] Srivastava N, Hinton G, Krizhevsky A, Sutskever I, Salakhutdinov R. Dropout: a simple way to prevent neural networks from overfitting. *Journal of Machine Learning Research*. 2014;15(1):1929-58.
- [46] Hush DR, Horne BG. Progress in supervised neural networks. *IEEE Signal Processing Magazine*. 2002;10(1):8-39.

- [47] Smith M. Neural Networks for Statistical Modeling: Van Nostrand Reinhold; 1993.
- [48] Hughes TJR, Cottrell JA, Bazilevs Y. Isogeometric analysis: CAD, finite elements, NURBS, exact geometry and mesh refinement. *Computer Methods in Applied Mechanics & Engineering*. 2005;194(39–41):4135-95.
- [49] Cottrell JA, Hughes TJR, Bazilevs Y. *Isogeometric Analysis: Toward Integration of CAD and FEA*: Wiley Publishing; 2009. 299-325 p.
- [50] Bazilevs Y, Hughes TJR. NURBS-based isogeometric analysis for the computation of flows about rotating components. *Computational Mechanics*. 2008;43(1):143-50.
- [51] Abedi R, Petracovici B, Haber RB. A space–time discontinuous Galerkin method for linearized elastodynamics with element-wise momentum balance. *Computer Methods in Applied Mechanics & Engineering*. 2006;195(25–28):3247-73.
- [52] Bazilevs Y, Calo VM, Cottrell JA, Hughes TJR, Reali A, Scovazzi G. Variational multiscale residual-based turbulence modeling for large eddy simulation of incompressible flows. *Computer Methods in Applied Mechanics & Engineering*. 2007;197(1–4):173-201.
- [53] Bazilevs Y, Calo VM, Hughes TJR, Zhang Y. Isogeometric fluid-structure interaction: theory, algorithms, and computations. *Computational Mechanics*. 2008;43(1):3-37.
- [54] Bazilevs Y, Calo VM, Zhang Y, Hughes TJR. Isogeometric Fluid–structure Interaction Analysis with Applications to Arterial Blood Flow. *Computational Mechanics*. 2006;38(4-5):310-22.
- [55] BAZILEVS Y, COTTRELL JA, HUGHES TJR, SANGALLI G. ISOGOMETRIC ANALYSIS: APPROXIMATION, STABILITY AND ERROR ESTIMATES FOR h-REFINED MESHES. *Mathematical Models & Methods in Applied Sciences*. 2006;16(07):1031-90.
- [56] Farin GE. *NURB curves and surfaces: from projective geometry to practical use*: A. K. Peters, Ltd.; 1995.
- [57] Sevilla R, Fernández-Méndez S. Numerical integration over 2D NURBS-shaped domains with applications to NURBS-enhanced FEM. *Finite Elements in Analysis*

& Design. 2011;47(10):1209-20.

- [58] Schillinger D, Hossain SJ, Hughes TJR. Reduced Bézier element quadrature rules for quadratic and cubic splines in isogeometric analysis. *Computer Methods in Applied Mechanics & Engineering*. 2014;277:1-45.
- [59] Antolin P, Buffa A, Calabrò F, Martinelli M, Sangalli G. Efficient matrix computation for tensor-product isogeometric analysis: The use of sum factorization. *Computer Methods in Applied Mechanics & Engineering*. 2015;285:817-28.
- [60] Hughes TJR, Reali A, Sangalli G. Efficient quadrature for NURBS-based isogeometric analysis ☆ . *Computer Methods in Applied Mechanics & Engineering*. 2010;199(5):301-13.
- [61] Auricchio F, Calabrò F, Hughes TJR, Reali A, Sangalli G. A simple algorithm for obtaining nearly optimal quadrature rules for NURBS-based isogeometric analysis. *Computer Methods in Applied Mechanics & Engineering*. 2012;s 249–252(2):15-27.